Applied Catalysis B: Environmental 168-169 (2015) 212–219

Contents lists available at ScienceDirect

Applied Catalysis B: Environmental

journal homepage: www.elsevier.com/locate/apcatb

Effect of Pt and Gd on coke formation and regeneration during JP-8 cracking over ZSM-5 catalysts

Sungtak Kim, Erdem Sasmaz, Jochen Lauterbach*

Smartstate Center for Strategic Approaches to the Generation of Electricity (SAGE), Department of Chemical Engineering, University of South Carolina, Columbia, SC 29201, USA

ARTICLE INFO

Article history:
Received 30 September 2014
Received in revised form
15 December 2014
Accepted 18 December 2014
Available online 20 December 2014

Keywords:
ZSM-5
Coke
Regeneration
Pt
Gd
JP-8
Cracking
LPG

ABSTRACT

Pt and Gd loaded ZSM-5 catalysts were synthesized by ion exchange method to investigate the effect of metal promoters on catalyst activity, coking and regeneration during military aviation fuel (JP-8) cracking into petroleum gas (PG) at 723 K. Multiple cracking and regeneration cycles were performed over the ZSM-5 based catalysts and their crystalline structure, oxidation profile, coke band and acidity were characterized. It was revealed that addition of Gd metal to the ZSM-5 catalyst prevented formation of complex aromatic coke and increased the number of Lewis acid sites, while Pt promoted ZSM-5 catalyst showed a decrease in the coke oxidation temperature. The effect of Pt and Gd promoters enhanced the coke burn-off ability, formed hydrogen rich carbon species and reduced oxidation temperature of coke substantially. Furthermore, agglomeration of Pt particles was partially impeded by coexisting Gd metal on the regenerated ZSM-5 catalyst. Synergetic effects of Pt and Gd promoters stabilized the PG yield and product distribution over the Pt–Gd/ZSM-5 catalyst during the cracking and regeneration cycles.

1. Introduction

Producing portable power from logistic hydrocarbon fuels, such as military aviation fuel (JP-8), kerosene, gasoline, or diesel is a critical need for current and future military and civilian applications. A fuel converter that can produce a mixture of lightweight hydrocarbons resembling liquefied petroleum gas (LPG) can be used as a practical and portable energy supply in rural settings, emergency response situations, sea expeditions, and military operations, where grid power is unreliable or unavailable. For instance, an LPG powered solid oxide fuel cell can provide higher gravimetric energy density, better thermal efficiency, lower noise and less emissions than a conventional internal combustion generator, while having longer operating time than batteries [1].

Extraction of petroleum gas (PG), consisting of C_2–C_4 hydrocarbon, from such fuels via catalytic cracking has drawn attention due to its distinct advantages as a mobile energy source with better flexibility and higher efficiency [2]. For practical applications, any catalyst used for cracking hydrocarbon fuels would need to handle high sulfur content in the fuel, resist coke formation for use in off-grid settings, and operate in a temperature range from 673 K to 873 K in order to decrease coke formation, energy consumption, and heat signature [3,4]. The fuel is not to be desulfurized before reaching to the catalyst, and only fuel and air can be injected to the reactor [5,6].

Zeolite catalysts have been used for hydro and catalytic cracking of hydrocarbons due to their high activity, shape selectivity, thermal stability and cation exchange capability [7–9]. Nevertheless, deactivation of zeolites by coke formation during hydrocarbon cracking is unavoidable due to the presence of longer-chain and aromatic hydrocarbon feed stock [3,10,11]. Although catalytic activity of zeolites during cracking reactions can be recovered with a regeneration treatment at high temperature, complex structured coke formed on the catalysts usually cannot be removed completely [3,10]. Numerous studies were performed to investigate the addition of metal promoters on zeolite catalysts in order to enhance their coke tolerance and regenerability as well as catalytic activity for hydrocarbon cracking. Noble metals, such as Ir, Pd, Pt, Rh, and Ru were reported to improve catalytic activity and reduce coking rate through dehydrogenation and hydrogenation [12–15]. In addition, rare earth metals were found to increase thermal stability and catalytic activity of zeolite catalysts by modifying their acid and base properties [16,17].

* Corresponding author at: 541 Main St, Room 135, Horizon I, Columbia, SC 29201, USA. Tel.: +1 803 777 7914; fax: +1 803 777 0973.
E-mail address: lauteraj@cec.sc.edu (J. Lauterbach).

http://dx.doi.org/10.1016/j.apcatb.2014.12.027
0926-3373/

Previously, a wide range of catalysts, ranging from metal promoted oxides to zeolite based catalysts were screened in our group for their JP-8 cracking activity using high-throughput experimentation [6]. The best bi-metallic promoted zeolite based catalysts were recommended for a secondary screening to evaluate their initial product distribution and effect of multiple regenerations on the product distribution. It was found that ZSM-5 catalysts with Si/Al ratios between 15 and 50 exhibited an outstanding performance at the temperature range of 673–823 K among other metal oxide and zeolite catalysts [6]. Pt and Gd promoted ZSM-5 catalysts showed enhanced regeneration capacity and elongated catalyst life time [5,6,18,19]. Here, Pt and Gd promoted ZSM-5 catalysts were investigated in detail to understand the effect of Pt–Gd on coke formation and catalyst regenerability during catalytic cracking of JP-8.

2. Experimental

2.1. Catalyst preparation

Pt/ZSM-5, Gd/ZSM-5 and Pt–Gd/ZSM-5 catalysts were prepared by ion exchange of a commercial ZSM-5 (Alfa Aesar: ammonium, SiO_2:Al_2O_3 = 50:1) with aqueous solutions of $Pt(NH_3)_4Cl_2{\cdot}H_2O$ (Alfa Aesar) and $Gd(NO_3)_3{\cdot}H_2O$ (Alfa Aesar). 0.1 M of aqueous solutions of Pt, Gd and Pt–Gd (50:50) were mixed with the commercial ZSM-5 with a ratio of 50 to 1. Ion exchange was accomplished under stirring at 353 K for 12 h. The ZSM-5 slurry was washed by de-ionized water and dried at 373 K. After three subsequent ion exchange processes, a final calcination step was performed in air for 3 h at 823 K to remove any residual precursor salt materials and oxidize the active metals.

2.2. JP-8 cracking activity measurements

The reactor for catalytic cracking of JP-8 consisted of a 0.5 inch o.d. quartz tube loaded with 150 mg of powder catalyst and was operated at 723 K under atmospheric pressure. JP-8 was fed into a stainless steel evaporator at 573 K by a peristaltic pump (Cole-Parmer, Masterflex L/S), and mixed with industrial grade He. The temperatures in the evaporator and reactor tube were monitored by thermocouples (type K, Omega). Weight hourly space velocity (WHSV, ratio of mass flow rate of JP-8 to weight of the catalyst) was 40 h^{-1}. The volumetric flow rate ratio of He to JP-8 at a reaction temperature of 723 K was 3.14. The effluent gas was passed through a chiller at 278 K to separate PG from unreacted JP-8 and heavier-chain hydrocarbons. The separated product stream was then injected directly to gas chromatography–mass spectrometry (GC–MS, Shimadzu QP 2010 Plus) equipped with a HayeSep-D capillary column (0.53 mm ID × 30 m; Agilent) using He as the carrier gas for analysis. PG yield was evaluated on a mass basis and defined as the sum of (kg C_2–C_4 out)/(kg JP-8 in). JP-8 cracking reactions were run multiple times and error ranges were calculated by the reiterated cracking reactions. Regeneration of the spent catalyst after each 10 h cracking reaction was performed by flowing 100 sccm of air over the catalyst bed at 723 K. JP-8 fuel, used in all experiments contained sulfur compounds up to 700 ppmw and its boiling point was in between 433 K and 553 K [20].

2.3. Catalyst characterization

Brunauer–Emmett–Teller (BET) surface area and pore volume of the ZSM-5 catalysts were measured by using automated gas adsorption system (NOVA 2000 or ASAP 2100, Micromeritics). The samples were kept at 423 K for 3 h under 1.0×10^{-6} Torr, and subsequently N_2 adsorption was performed at 77 K.

The amount of metal loading on the ZSM-5 catalysts after ion exchange was measured using an Inductively Coupled Plasma–Optical Emission Spectrometer (ICP–OES, PerkinElmer Optima 2000 DV). The metal solutions were prepared as follows: 50 mg of catalysts was mixed with 1 g of sodium peroxide (Na_2O_2, Sigma–Aldrich) in a zirconium crucible and heated by a Bunsen burner until the catalyst and the Na_2O_2 completely melted and mixed. After cooling down the crucible to get a white slurry of the catalyst and the Na_2O_2 mixture, the slurry was digested by 3 mL of HNO_3 (70%, Alfa Aesar) and 9 mL of HCl (38%, Alfa Aesar), then heated at 393 K for 3 h. After complete dissolution, the obtained solution was transferred into a 100-mL calibrated flask that was finally filled with deionized water.

Temperature programmed oxidation (TPO) was performed to determine coke burn-off temperatures of the spent catalyst samples collected after 10 h JP-8 cracking reaction at 723 K. The measured CO_2 content as a function of temperature provides information about the onset and extent of coke burn-off. All TPO measurements were obtained using a quadrupole mass spectrometer equipped with a fast response inlet capillary/leak valve system and a heating apparatus with 25 mg of sample loaded in a quartz tube. The spent catalysts were pretreated with He at 473 K for drying and removal of volatile compounds before the oxidation step. The system was heated at a ramping rate of 20 K/min under 10 sccm flow of 10% O_2 with balance He.

IR spectra of the spent catalysts were recorded using a FTIR spectrometer equipped with a mercury–cadmium–telluride-B detector (Nicolet Nexus 4700). The spectra were collected in single beam absorbance mode with a spectral resolution of 4 cm^{-1} at room temperature. 20 mg of catalyst samples were prepared as self-supporting pellets with a diameter of 12 mm and placed in a stainless steel variable temperature gas flow transmission cell, which has two IR-transparent NaCl windows. The catalyst was pretreated at 473 K for 3 h under flowing He. The temperature of the cell was monitored by a thermocouple (type K, Omega) located near to the pellets.

Powder X-ray diffraction (XRD) was used to determine crystallinity and cell parameters for the catalyst samples. A Rigaku Miniflex II powder X-ray diffractometer was used for bulk phase analysis of the catalysts. A Cu Kα source with 1.54 Å wavelength was used. The voltage was set to 45 kV and current to 40 mA. All spectra were collected at 2θ values between 3° and 80° using a step size of 0.02° and 2 s per step. Crystallinity of the samples was defined as the ratio of intensity from crystalline peaks to the sum of the crystalline and amorphous peak intensities.

Pyridine adsorption experiments were conducted in the same IR cell described above. After pretreatment, pyridine vapor was flowed into the transmission cell at 423 K for 30 min to ensure all acid sites on the catalyst surface were covered by pyridine. Then, the catalyst pellets were kept under He flow at 423 K for 30 min to remove any physically adsorbed pyridine before the IR spectra were taken. The IR spectra of adsorbed pyridine were recorded from 1400 cm^{-1} to 1700 cm^{-1}, and both chemisorbed pyridinium ion (PyH^+) on Brönsted acid sties and pyridine bonded on Lewis acid sites (PyL) were quantified at 1450 cm^{-1} and 1545 cm^{-1}, respectively. The extinction coefficients of PyH^+ (1545 cm^{-1}) and PyL (1450 cm^{-1}) were taken to be 1.13 cm/μmol (PyH^+) and 1.28 cm/μmol (PyL), respectively [21].

Scanning transmission electron microscopy–energy dispersive X-ray spectroscopy (STEM–EDX) was used to image the materials with a JEOL 2100F 200 kV FEG–STEM/TEM equipped with a CEOS Cs corrector on the illumination system. The geometrical aberrations were measured and controlled to provide less than a $\pi/4$ phase shift of the incoming electron wave over the probe-defining aperture of 17.5 mrad which at 200 kV provides a nominal probe size of <0.1 nm. High angle annular dark-field (HAADF) STEM images were acquired on a Fischione Model 3000HAADF detector with a spanning angle of 50–284 mrad. The scanning acquisition was

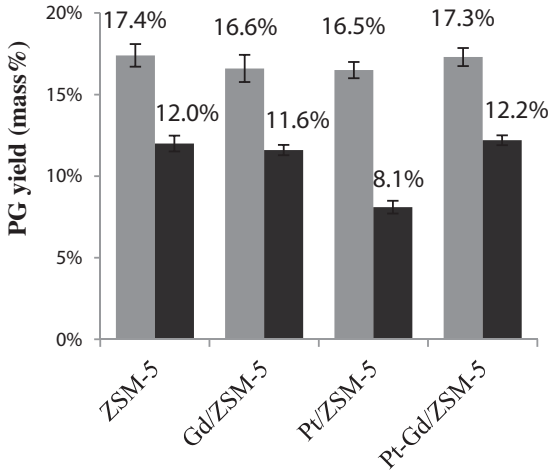

Fig. 1. PG yields from JP-8 cracking at 723 K after 1 h (grey) and 10 h (black) TOS of the base ZSM-5 and the metal promoted ZSM-5 catalysts.

synchronized to the 60 Hz AC electrical power to minimize 60 Hz noise in the images and a pixel dwell time of 15.8 μs was chosen. Scanning electron microscopy (SEM) images and EDX of the ZSM-5 catlaysts were obtained using a Zeiss Ultraplus Thermal Field Emission Scanning Electron Microscope with an acceleration voltage of 15 kV.

3. Results and discussion

3.1. Cracking performance of the ZSM-5 based catalysts

Textural properties of the ZSM-5 catalysts and metal loadings of the Pt and Gd promoted ZSM-5 catalysts are shown in Table 1. Crystal size of the ZSM-5 catalysts ranged from 150 nm to 220 nm, based on the analysis of SEM images. The Pt loading was found to be 3.76%, whereas the Gd loading was remained below 0.52% on the ZSM-5 catalysts. PG yields over the base and metal promoted ZSM-5 catalysts during JP-8 cracking were determined at a reactor temperature of 723 K at 1 and 10 h time-on-stream (TOS). As shown in Fig. 1, PG yields over the base ZSM-5 catalyst were found to be 17.4% (±0.7) and 12.0% (±0.5) at 1 and 10 h TOS, respectively. None of the metal loaded ZSM-5 catalysts showed higher initial cracking activity in comparison to that of the base ZSM-5 catalyst. The Pt/ZSM-5 catalyst was found to have the lowest PG yield (8.1% ±0.4) after 10 h TOS, whereas addition of 0.5 wt% Gd to the Pt/ZSM-5 catalyst retained the PG yield to 12.2% (±0.3).

Initial product distribution of C_2–C_4 hydrocarbons produced on a mass basis during JP-8 cracking over the ZSM-5 catalysts at 723 K is shown in Fig. 2. Propane and propylene were found to be the dominant products over all catalysts. Both the base and Pt promoted ZSM-5 catalysts showed a similar product distribution after 1 h TOS. The paraffin to olefin ratio (P/O) over the Gd/ZSM-5 catalyst was determined to be the lowest among the ZSM-5 based catalysts. The effect of Gd and Pt on the product selectivity indicated that more olefin compounds were produced over the Gd/ZSM-5 catalyst whereas more paraffin compounds were produced over the Pt/ZSM-5 catalyst.

The average PG yield from JP-8 cracking over the ZSM-5 based catalysts at 723 K after multiple 10 h cracking and regeneration cycles was measured to investigate catalyst regenerability. As shown in Fig. 3, the average PG yield over the base ZSM-5 catalyst decreased by 52% after the 5th cracking and regeneration cycle. Addition of Gd to the ZSM-5 catalyst did not improve the average PG yield after multiple cracking and regeneration cycles. In the case of the Pt/ZSM-5 catalyst, the average PG yield remained stable for the first four cracking cycles and slightly decreased in the last two ones. Although the average PG yield over the Pt/ZSM-5 catalyst remained 31% higher than that over the base ZSM-5 catalyst in the last cracking cycle, the original catalytic activity could not be recovered completely. In contrast, the bimetallic Pt–Gd promoted ZSM-5 catalyst exhibited a stable activity with an average PG yield of 15%, and its initial activity was recovered by 98% after the 5th cracking and regeneration cycle.

The selectivity to C_2–C_4 hydrocarbons over the ZSM-5 based catalysts at 723 K at 1 h TOS after the 5th cracking and regeneration cycle is shown in Fig. 4. An effect of multiple regenerations and cracking cycles on the product distribution was clearly observed over the base and Gd promoted ZSM-5 catalysts. In comparison to the product distribution of the fresh ZSM-5 catalysts shown in Fig 2, the selectivity of C_3 and C_4 hydrocarbons over the base and Gd promoted ZSM-5 catalysts changed at 1 h TOS after the 5th cracking and regeneration cycle, leading to a decrease of their P/O ratio to 44.6% and 46.8%, respectively. In addition, the initial selectivity towards propane over Pt/ZSM-5 decreased to 24.4%, whereas that to 1-butene increased to 18.4% at 1 h TOS after the 5th cracking and regeneration cycle. These changes resulted in a 13.3% decrease of the P/O ratio over the regenerated Pt/ZSM-5 catalyst in comparison to that over the fresh catalyst. The product selectivity over the bimetallic Pt–Gd promoted ZSM-5 catalyst remained unchanged after the 5th cracking and regeneration cycle, indicating that the presence of Pt and Gd on the ZSM-5 catalyst influenced catalyst deactivation, selectivity and regeneration. The diminished performance of the ZSM-5, Gd/ZSM-5 and Pt/ZSM-5 catalysts can be attributed to either its inability to perform coke burn-off at the given temperature (723 K) or a fundamental degradation, such as loss of acid sites or crystallinity by dealumination of the catalyst [22–24], which are discussed in the following sections.

3.2. Durability of the ZSM-5 based catalysts

The XRD patterns of the fresh and regenerated catalysts after the 5th cracking and regeneration cycle at 723 K are shown in Fig. 5. All of the fresh catalysts exhibited characteristic diffraction peaks of the mordenite framework inverted (MFI) structure at $2\theta = 23.12^\circ$ (332), 23.30° (051), 23.74° (151), and 23.96° (3 0 3), indicating orthorhombic structure with high crystallinity (>96%).

Table 1
Textural properties and metal loading of the Gd and Pt promoted ZSM-5 catalysts.

	S_{BET} (m^2/g)	$S_{external}$ (m^2/g)	V_{Total} (cm^3/g)	Metal loading (wt%)	
				Gd	Pt
ZSM-5	287	0.032	203	N/A	N/A
Gd/ZSM-5	285	0.038	207	0.52% (±0.05)	N/A
Pt/ZSM-5	291	0.046	175	N/A	3.52% (±0.35)
Pt–Gd/ZSM-5	287	0.044	181	0.46% (±0.06)	3.76% (±0.5)

A maximum error range of S_{BET}, $S_{external}$, and V_{Total} is of the ZSM-5 catalysts is ±6%.
Standard deviation of each metal loading is shown in parenthesis.

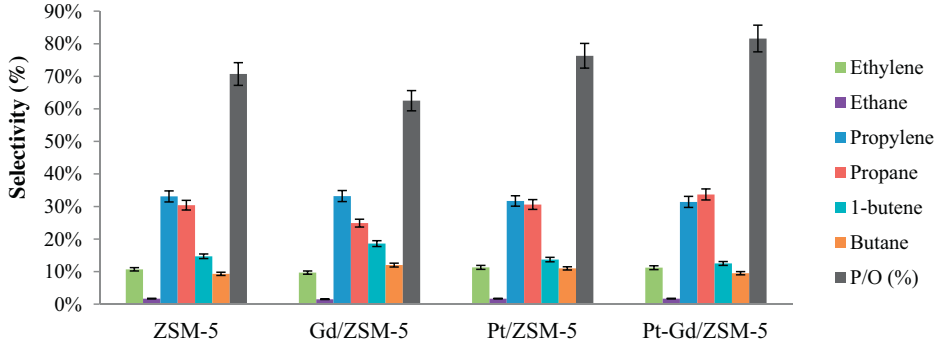

Fig. 2. Initial selectivity of the fresh ZSM-5 based catalysts at 723 K after 1 h TOS.

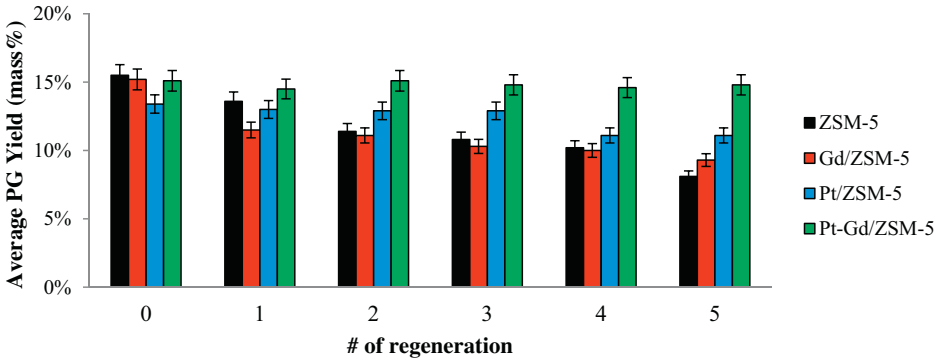

Fig. 3. Average PG yield from JP-8 cracking of the ZSM-5 catalysts at 723 K after multiple 10 h JP-8 cracking reaction and regeneration cycles.

Characteristic diffraction peaks of the fresh ZSM-5 catalysts shifted to lower 2θ values (by about 0.2°) with Gd and Pt promotion, showing that metals are ion exchanged into the ZSM-5 framework [25]. The XRD peaks at 23.12° and 23.30° appeared as a single peak at 23.12° (3 3 2) for the regenerated base ZSM-5 and Gd/ZSM-5 catalysts indicating that their crystalline structures changed and appeared as a tetragonal structure after the cracking and regeneration cycles. These results are consistent with the literature in which the crystalline structure of ZSM-5 (SiO_2:Al_2O_3 = 54) changed from orthorhombic to tetragonal structure after catalytic reaction of C_4 hydrocarbon at 673 K due to the coke deposits formed on the ZSM-5 catalysts [22]. Although the regenerated Pt/ZSM-5 catalyst remained as orthorhombic structure, a phase shift was observed for the peaks at 22.98°, 23.19°, 23.6° and 23.83°. However, the bimetallic Pt–Gd promoted ZSM-5 catalyst did not indicate a peak shift and its crystallinity remained unchanged after the cracking and regeneration cycles.

3.3. Morphology of Pt and Gd loaded ZSM-5

STEM images of the fresh and regenerated Pt/ZSM-5 and Pt–Gd/ZSM-5 catalysts after the 5th cracking and regeneration cycle at 723 K were collected to determine particle size distribution and morphology of Pt and Gd loaded ZSM-5 catalysts before and after the cracking and regeneration cycles. Although Pt was synthesized via an ion-exchange method, Pt nanoparticles formed on the catalyst due to the higher Pt loading and/or lack of thermal stability of Pt on the zeolite [12,25]. Sintering of Pt at temperatures above 573 K, regardless of catalyst synthesis methods, was previously reported [25,26]. As shown in Fig. 6, all bright particles represent Pt nanoparticles on the fresh and regenerated samples based on the elemental analysis obtained from STEM–EDX. Further STEM–EDX analysis revealed that Gd was not found on the Pt nanoparticles and bimetallic formation of Pt–Gd nanoparticles was not observed within the limitations of the instrument. It is possible

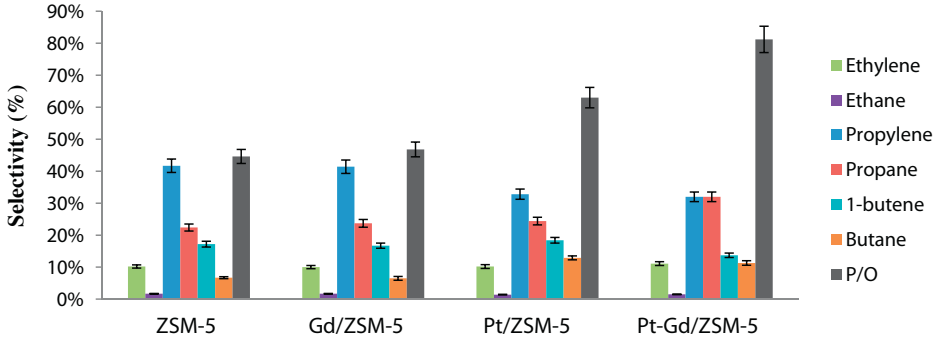

Fig. 4. Initial selectivity of the ZSM-5 based catalysts after the 5th cracking and regeneration cycle at 723 K after 1 h TOS.

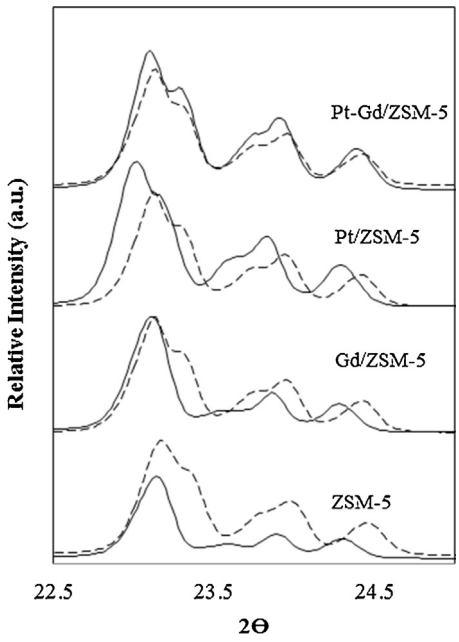

Fig. 5. XRD patterns of the fresh (dashed lines) and regenerated (solid lines) ZSM-5 based catalysts after the 5th cracking and regeneration cycle at 723 K.

that STEM–EDX spectral peaks of Gd could not be detected due to the low Gd metal loading (0.46%) and sensitivity limits of the instrument. However, analysis of the fresh Gd/ZSM-5 and Pt–Gd/ZSM-5 catalysts using SEM–EDX revealed presence of Gd and showed that no Gd nanoparticles were visible on any of these samples (Supplementary data 1). Both Pt and Gd metals were uniformly distributed on the ZSM-5 support based on SEM–EDX mapping (Supplementary data 2).

Particle size distribution of the Pt loaded ZSM-5 catalysts were calculated, as shown in Fig. 6A and B. The average Pt particle sizes of the fresh Pt/ZSM-5 and Pt–Gd/ZSM-5 catalysts were found to be 7.2 nm and 7.3 nm, respectively. In both samples, 30% of the Pt particles were found to be smaller than 2 nm and the rest of them distributed in between 5 nm and 20 nm. After the regeneration, the average Pt particle size of the Pt/ZSM-5 and Pt–Gd/ZSM-5 catalysts increased to 11.2 nm and 11.3 nm, respectively. Furthermore, the Pt particle size of the regenerated Pt/ZSM-5 catalyst mostly distributed in between 5 and 15 nm, but no small particles (<2 nm) were observed. In contrast, 8% of Pt particles on the regenerated Pt–Gd/ZSM-5 catalyst still remained to be smaller than 2 nm, resulting in the broad size distribution from 0.5 nm up to 20 nm. (Fig. 6C and D).

It is generally known that Pt particles tend to agglomerate at temperatures above 573 K and start to move on support materials with increasing reduction temperature [27,28]. Nevertheless, it is clear that sintering of Pt particles was less significant on the Pt–Gd/ZSM-5 catalyst, and one possible reason could be the existence of Gd atoms, influencing the electronic potential around Pt [16,29]. In addition, shapes of the Pt nanoparticles were found to change with Gd promotion on the regenerated samples, as shown in Fig. 6E and F. Pt particles on the regenerated Pt/ZSM-5 catalyst had cuboctahedral shapes with truncated corners, whereas those on the regenerated Pt–Gd/ZSM-5 catalyst had mostly cuboctahedral shapes. The different Pt particle shapes were previously reported to affect the product distribution strongly during the benzene hydrogenation reaction [30], which was also observed during JP-8 cracking in this work.

3.4. Effect of metal on coke formation and burn-off

The coke deposits and carbon content formed during the cracking reactions were further analyzed via TPO. The TPO profiles of

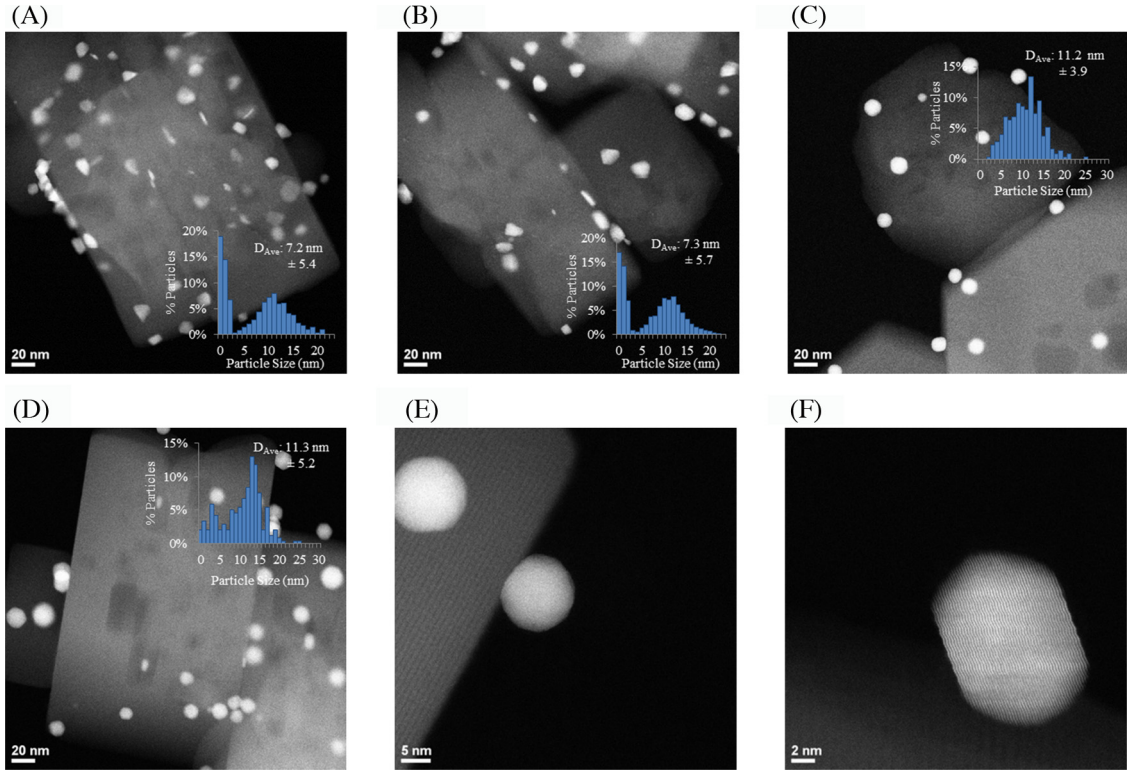

Fig. 6. STEM images of fresh Pt/ZSM-5 (A), fresh Pt–Gd/ZSM-5 (B), regenerated Pt/ZSM-5 (C), regenerated Pt–Gd/ZSM-5 (D), the particle shapes; regenerated Pt/ZSM-5 (E) and regenerated Pt–Gd/ZSM-5 (F).

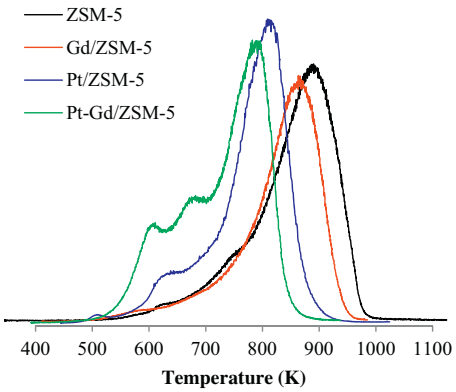

Fig. 7. TPO profiles of the spent catalysts after JP-8 cracking for 10 h TOS at 723 K.

coke deposits over the ZSM-5 based catalysts, collected after 10 h of cracking reaction at 723 K, are shown in Fig. 7. The maximum oxidation temperature obtained over the base ZSM-5 catalyst (891 K) shifted towards lower temperatures as the catalyst promoted with metals. For instance, the maximum oxidation temperatures of the Gd/ZSM-5, Pt/ZSM-5 and Pt–Gd/ZSM-5 catalysts were found be at 856 K, 790 K, and 765 K, respectively. In addition, shoulder peaks observed for the Pt/ZSM-5 (621 K) and Pt–Gd/ZSM-5 catalysts (597 K and 664 K) correspond to coke formed on the metal, or metal and zeolite interface [31–34]. The area of the shoulder peaks obtained from the spent Pt–Gd/ZSM-5 catalyst was found to be larger in comparison to that from the spent Pt/ZSM-5 catalyst, indicating that more coke could be oxidized at lower temperature on the Pt–Gd/ZSM-5 catalyst. High coke oxidation capability of the Pt–Gd/ZSM-5 catalyst resulted in a stable average PG yield throughout the cycles (Fig. 3), and the larger shoulder peak area in the TPO profile of the spent Pt–Gd/ZSM-5 catalyst could be attributed to the higher Pt particle dispersion (Fig. 6), consistent with the SEM images. Since both TPO profile and SEM images indicated that Pt was dispersed throughout the zeolite as particles, the dispersed Pt particles could be responsible for improving the coke burn-off properties of the catalyst. In addition, these results are in good agreement with the thin-film optical screening experiments in which Pt–Gd thin film alloys on the pressed MFI structure zeolite illustrated less coke formation due to the presence of Gd [19].

Carbon content and H/C ratio of the coke deposits formed on the ZSM-5 based catalysts after 10 h TOS of JP-8 cracking at 723 K were determined by measuring the total amount of H_2O, CO, and CO_2 released during the TPO experiments. As shown in Table 2, carbon content of the coke deposits on the spent Gd/ZSM-5 and base ZSM-5 catalysts were similar to each other, while Pt/ZSM-5 and Pt–Gd/ZSM-5 catalysts showed 53% and 44% more carbon content than that on the spent ZSM-5 catalyst, respectively. In addition, H/C ratio of the spent Pt/ZSM-5 catalyst was calculated to be 0.98 indicating that less hydrogen rich carbon species, such as aliphatic carbons or less complex aromatics, formed on the catalyst during the JP-8 cracking reaction. Promotion of Gd to the base ZSM-5 and Pt–ZSM-5 catalysts increased the H/C ratio up to 1.36.

Table 2
Carbon content (wt%), H/C ratio, and IR peak intensity ratio of the spent ZSM-5 based catalysts after JP-8 cracking for 10 h TOS at 723 K.

	Carbon content[a] (wt%)	H/C Ratio[a]	$I_{CH(CH2)}/I_{CH3}$[b]	I_{coke}/I_{CC}[b]
ZSM-5	8.9 (±0.4)	1.29 (±0.09)	1.32	0.81
Gd/ZSM-5	8.7 (±0.6)	1.35 (±0.1)	0.71	0.51
Pt/ZSM-5	13.6 (±1.0)	0.98 (±0.04)	1.25	0.87
Pt–Gd/ZSM-5	12.8 (±0.7)	1.36 (±0.07)	0.95	0.75

[a] Carbon content (wt%), H/C ratio were obtained from TOS experiment.
[b] IR peak intensity ratio; at 2927 cm^{-1}(—CH(CH2)) to 2970 cm^{-1}(—CH3) and at 1598 (coke) cm^{-1} to 1620 cm^{-1}(C=C).

FT-IR spectroscopy on the ZSM-5 based catalysts collected after 10 h of JP-8 cracking at 723 K was carried out in order to identify the coke deposits. IR spectra shown in Fig. 8A correspond to CH stretching vibrations of paraffinic species for the spent ZSM-5 catalyst. The bands at around 2960–2970 cm^{-1} and 2870 cm^{-1} are associated with —CH_3 groups, while those at 2927 cm^{-1} and 2858 cm^{-1} are associated with asymmetric and symmetric —$CH(CH_2)$ groups, respectively [35–37]. FT-IR spectra in Fig. 8B, on the other hand, show the C=C stretching vibration of unsaturated hydrocarbons at 1620 cm^{-1} and the C—H bending vibration of complex aromatic molecules, the so-called "coke band" at 1598 cm^{-1} [32,35–37]. Besides the peak identification, a relative length of aliphatic carbon and complex aromatic molecules can be determined by taking ratios of the peak intensities of —$CH(CH_2)$ groups to —CH_3 groups and coke band to C=C, respectively. As shown in Table 2, longer aliphatic carbon species and less complex aromatic molecules formed on the spent Gd/ZSM-5 and Pt–Gd/ZSM-5 catalysts. Furthermore, the broad and low intensity peak observed on the spent Gd/ZSM-5 at 2927 cm^{-1} and 2858 cm^{-1} implied that Gd prevented formation of carbon double bond in aliphatic structured coke.

The shift of the oxidation temperature in the TPO profile can be a clear evidence of Gd and Pt effect on coke burn-off. In accordance with analogous investigations about coke characterization on various Pt loaded catalysts, oxidation of the coke deposits can be catalyzed on the Pt promoted catalysts due to the high reactivity of Pt to O_2, resulting a decrease in the oxidation temperature [31–34]. Furthermore, Pt particles on the ZSM-5 catalysts promoted dehydrogenation of hydrocarbon intermediates to form aromatic structured coke, resulting in the formation of complex aromatic structured coke compounds, such as methylpyrenes, and more carbon content on the zeolite [10,38,39]. Although more coke was formed over the Pt promoted catalysts, TPO profiles proved that those catalysts possessed better coke burn-off ability than non Pt promoted catalysts. On the other hand, Gd modified the hydrogenation activities and the acid properties of the catalysts [40–42]. Additional Lewis acid sites originated by Gd cations in the ZSM-5 catalysts could lead to a decrease in the oxidation temperature of coke [42,43]. In addition, the presence of Gd hindered formation of the complex aromatic structured coke on the catalyst surface and prevent further aromatization by increasing basicity of zeolite catalyst [16]. Therefore, the coke burn-off ability of Pt–Gd/ZSM-5 catalysts is apparently improved by coexistence of Pt and Gd, leading to lowering the coke burn-off temperature, forming hydrogen rich coke structure, and suppressing formation of the complex aromatic structured coke.

3.5. *Effect of acidity to the ZSM-5 based catalysts*

Acidity of a zeolite catalyst is one of the controlling factors that determine its catalytic activity and selectivity. Acidity and catalytic activity can be modified by addition of metal atoms to the supported zeolite pore structure [12,15,44]. For instance, it was reported that paraffin species were more likely produced via the direct attack of the proton on a C—C bond, which could be provided by Brönsted acid sites, whereas Lewis acid sites could extract the hydride ion from paraffin molecules and form carbenium ion, thus olefin products [16,45–47]. To determine the effect of Brönsted and Lewis acid sites on the fresh, spent (collected after the 10 h TOS), and regenerated (collected after 5th cracking and regeneration cycle) ZSM-5 based catalysts, pyridine adsorption and desorption experiments were conducted at 423 K and the amount of acid sites on those catalysts were calculated, as shown in Table 3.

It was determined that the number of Lewis acid sites on the fresh Gd/ZSM-5 and Pt–Gd/ZSM-5 catalysts increased by 40% and

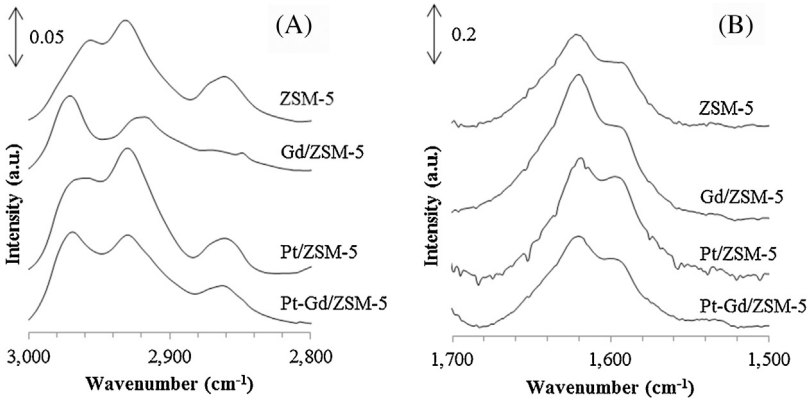

Fig. 8. IR spectra of the spent ZSM-5 based catalysts after JP-8 cracking for 10 h TOS at 723 K: (A) region 2800–3000 cm^{-1}, (B) region 1500–1700 cm^{-1}.

58%, respectively, in comparison to that on the fresh ZSM-5 catalyst. Modification of the ZSM-5 catalyst with Gd created new Lewis acid sites by substituting the framework protons with Gd^{3+} cations [48]. The increase in Lewis acid sites on the Gd/ZSM-5 and Pt–Gd/ZSM-5 catalysts indicated that Gd was ion-exchanged as Gd^{3+}cations. It was expected that if any Gd was dispersed as particles on the surface, it would form Gd_2O_3 after high temperature calcination (823 K for 3 h with air). However, in that case the number of Lewis acid sites should not change, since Gd_2O_3 could not generate any acid sites [49].

Both the number of Brönsted and Lewis acid sites decreased significantly on all the spent catalysts after 10 h of reaction. Among the spent catalysts, the total number of acid sites decreased the most on the Pt/ZSM-5 catalyst, leading to the lowest PG yield after 10 h TOS, as shown in Fig. 2. It is important to note that this decrease is consistent with the high carbon content and low H/C ratio found on the Pt/ZSM-5 catalyst. After multiple cracking and regeneration cycles, Brönsted and Lewis acid sites could not be recovered completely on the base ZSM-5 and Gd/ZSM-5 catalysts due to the coke deposit formed on the catalysts. However, due to the improved coke burn-off performance of the Pt, the Pt promoted catalysts showed better regenerability, indicating that 89% of the total number of acid sites was recovered after the 5th cracking and regeneration cycle.

Although the number of Brönsted and Lewis acid sites on the Pt/ZSM-5 catalyst did not change much with the addition of Pt, the resulting product contained more paraffin compounds, as shown in Fig. 2. It was possible that Pt promotion enhanced the hydrogenation function of the solid acid catalysts, forming more paraffin compounds [50,51]. On the other hand, over the regenerated base ZSM-5, Gd/ZSM-5 and Pt/ZSM-5 catalysts, dealumination could lead to the formation of an extra framework aluminum which might decrease the number of strong Brönsted acid sites and limit the access of reactants to the acid sites, resulting in a PG yield with more olefin fraction, as shown in Table 3 [52]. Addition of Gd to the Pt/ZSM-5 catalysts improved the hydrogenation function of Pt, therefore, the highest P/O with the highest propane fraction was obtained over the Pt–Gd/ZSM-5 catalyst at 723 K. A similar behavior was also reported by Martins et al., where the presence of rare earth elements located close to the Pt clusters improved the hydrogenation activity of PtRE/HMCM-22 and PTRE/HBEA catalysts during isomerization of *n*-hexane [40]. In summary, synergetic effects of Pt and Gd promoters improved the coke burn off ability and modified the acidity of the ZSM-5 based catalysts, leading to stabilization of the PG yield and product distribution over the Pt–Gd/ZSM-5 catalyst after the 5th cracking and regeneration cycle by maintaining the initial acidity of the catalysts.

Table 3
Amount of Brönsted and Lewis acid sites determined by pyridine adsorption for the fresh and spent ZSM-5 based catalysts.

Samples	Acid sites on fresh catalysts ($\mu mol\ g^{-1}$)			Acid sites on spent catalysts ($\mu mol\ g^{-1}$)			Acid sites on regenerated catalysts ($\mu mol\ g^{-1}$)		
	B	L	L/B	B	L	L/B	B	L	L/B
ZSM-5	151	65	0.43	59	22	0.37	101	27	0.27
Gd/ZSM-5	142	91	0.64	65	25	0.36	75	36	0.48
Pt/ZSM-5	153	52	0.31	21	16	0.76	123	59	0.47
Pt–Gd/ZSM-5	152	103	0.68	65	17	0.26	128	98	0.77

A maximum error range for the catalysts' acidity is ±7.

4. Conclusion

Catalytic activity, coking, and regenerability of the bimetallic Pt–Gd promoted ZSM-5 catalysts were investigated during JP-8 cracking at 723 K. It was revealed that Pt and Gd played a different role in JP-8 cracking and the catalyst regeneration. Gd promotion of the ZSM-5 catalyst resulted in more hydrogen rich coke formation after 10 h TOS by preventing development of complex aromatic structured compounds. In addition, Gd increased the number of Lewis acid sites, which enhanced formation of the olefinic products during JP-8 cracking. On the other hand, addition of Pt to the ZSM-5 catalyst significantly decreased the coke oxidation temperature while catalyzing formation of the paraffin products. Coexistence of Gd and Pt resulted in higher Pt particle dispersion by still possessing small Pt nanoparticles (<2 nm) after the multiple cracking and regeneration cycles. Due to the synergetic effects of Pt and Gd promoters, the Pt–Gd/ZSM-5 catalyst showed the best cracking and regeneration performance with a stable PG yield and its acidity was mostly recovered after the 5th cracking and regeneration cycle.

Acknowledgments

The authors acknowledge the Defense Advanced Research Projects Agency (contract no. W91CRB-10-1-0007), and the South Carolina Smart State Center of Economic Excellence for Strategic Approaches to the Generation of Electricity for funding. We thank Dr Christopher T. Williams, Dr John R. Regalbuto, and Dr John R. Monnier for using FT-IR, ICP–OES, and TPO instruments, respectively.

Appendix A. Supplementary data

Supplementary data associated with this article can be found, in the online version, at http://dx.doi.org/10.1016/j.apcatb.2014.12.027.

References

[1] C. Song, Catal. Today 77 (2002) 17–49.
[2] L.Q. Maurice, H. Lander, T. Edwards, W.E. Harrison, Fuel 80 (2001) 747–756.
[3] M. Guisnet, L. Costa, F.R. Ribeiro, J. Mol. Catal. A: Chem. 305 (2009) 69–83.
[4] M. Guisnet, P. Magnoux, Stud. Surf. Sci. Catal. 88 (1994) 53–68.
[5] J. Lauterbach, M. Glascock, J. Bedenbaugh, C. Chang-Yin, A. Jangam, U.S. Patent 2013/0041198 A1 (2013).
[6] J. Bedenbaugh, S. Kim, E. Sasmaz, J. Lauterbach, ACS. Comb. Sci. 15 (2013) 491–497.
[7] H.A. Abrevaya, Suheil, in: S. Kulprathipanja (Ed.), Zeolites in Industrial Separation and Catalysis, Wiley-VCH, Weinheim, 2010, pp. 403–566.
[8] M. Rigutto, in: J.i.C.e.A.C.S. Zones (Ed.), Zeolites and Catalysis: Synthesis, Reactions and Applications, Wiley-VCH, Weinheim, 2010, pp. 547–585.
[9] G.T. Kokotailo, S.L. Lawton, D.H. Olson, D.H. Olson, W.M. Meier, Nature 272 (1978) 437–438.
[10] M. Guisnet, P. Magnoux, Appl. Catal. A 212 (2001) 83–96.
[11] M. Guisnet, P. Magnoux, Appl. Catal. 54 (1989) 1–27.
[12] J. Scherzer, A.J. Gruia, Hydrocracking Science and Technology, Marcel Dekker, New York, 1996.
[13] A. Funez, A. De Lucas, P. Sanchez, M.J. Ramos, J.L. Valverde, Chem. Eng. J. 136 (2008) 267–275.
[14] H.F. Wallace, K.E. Hayes, J. Catal. 29 (1973) 83–91.
[15] S. Sivasanker, K.J. Waghmare, K.M. Reddy, A.N. Kothasthane, P. Ratnasamy, J. Chem. Technol. Biotechnol. 48 (1990) 261–268.
[16] X. Wang, C. z. Zhao, Xu, D. Aijun, L. Zhang, J. Guiyuan, J. Rare Earth 25 (2007) 321–328.
[17] G. de la Puente, E.F. Souza-Aguiar, F.M.Z. Zotin, V.L.D. Camorim, U. Sedran, Appl. Catal. A 197 (2000) 41–46.
[18] J. Bedenbaugh, Investigation of Catalytic Materials for Cracking of Military Aviation Fuel to Liquefied Petroleum Gas: High Throughput Experimentation, Chemical Engineering, University of Delaware, 2012, pp. 77–186.
[19] K. Yang, J. Bedenbaugh, H. Li, M. Peralta, J.K. Bunn, J. Lauterbach, J. Hattrick-Simpers, ACS Comb. Sci. 14 (2012) 372–377.
[20] I.C. Lee, H.C. Ubanylonwu, Fuel 87 (2008) 312–318.
[21] M. Guisnet, P. Ayrault, J. Datka, Pol. J. Chem. 71 (1997) 1455–1461.
[22] A.G. Alvarez, H. Viturro, R.D. Bonetto, Mater. Chem. Phys. 32 (1992) 135–140.
[23] M.A. Kuehne, H.H. Kung, J.T. Miller, J. Catal. 171 (1997) 293–304.
[24] G.F. Froment, J. Demeyer, E.G. Derouane, J. Catal. 124 (1990) 391–400.
[25] M. Rivallan, E. Seguin, S. Thomas, M. Lepage, N. Takagi, H. Hirata, F. Thibault-Starzyk, Angew. Chem. Int. Ed. 49 (2010) 785–789.
[26] Y. Yamasaki, M. Matsuoka, M. Anpo, Catal. Lett. 91 (2003) 111–113.
[27] J.G.A.J. Scherzer, Hydrocracking Science and Technology, Marcel Dekker, New York, 1996.
[28] S.A. Bradley, W. Sinkler, D.A. Blom, W. Bigelow, P.M. Voyles, L.F. Allard, Catal. Lett. 142 (2012) 176–182.
[29] S. Jongpatiwut, P. Sackamduang, T. Rirksomboon, S. Osuwan, W.E. Alvarez, D.E. Resasco, Appl. Catal. A 230 (2002) 177–193.
[30] K.M. Bratlie, H. Lee, K. Komvopoulos, P.D. Yang, G.A. Somorjai, Nano Lett. 7 (2007) 3097–3101.
[31] N.S.F.J.M. Parera, E.M. Traffano, J. Catal. 79 (1983) 481–484.
[32] N. Martı, M. Viniegra, E. Lima, G. Espinosa, Ind. Eng. Chem. Res. 43 (2004) 1206–1210.
[33] J. Barbier, P. Marecot, R. Maurel, N. J. Chem. 4 (1980) 385–388.
[34] A.W. Chester, A.B. Schwartz, W.A. Stover, J.P. Mcwilliams, Chem. Technol. 11 (1981) 50–58.
[35] P. Castaño, G. Elordi, M. Olazar, A.T. Aguayo, B. Pawelec, J. Bilbao, Appl. Catal. B 104 (2011) 91–100.
[36] J. Pater, F. Cardona, C. Canaff, N.S. Gnep, G. Szabo, M. Guisnet, Ind. Eng. Chem. Res. 38 (1999) 3822–3829.
[37] H.G. Karge, W. Niessen, H. Bludau, Appl. Catal. A 146 (1996) 339–349.
[38] F. Zaera, G.A. Somorjai, J. Am. Chem. Soc. 106 (1984) 2288–2293.
[39] Z. Paal, R. Schlogl, G. Ertl, J. Chem. Soc. Faraday Trans. 88 (1992) 1179–1189.
[40] A. Martins, J.M. Silva, F.R. Ribeiro, M.F. Ribeiro, Stud. Surf. Sci. Catal. 158 (2005) 1875–1882.
[41] A. Barrera, M. Viniegra, S. Fuentes, G. Diaz, Appl. Catal. B 56 (2005) 279–288.
[42] J. Scherzer, R.E. Ritter, Ind. Eng. Chem. Res. 17 (1978) 219–223.
[43] H. Hirai, T. Masui, N. Imanaka, G. Adachi, J. Alloys Compd. 374 (2004) 84–88.
[44] N. Rahimi, R. Karimzadeh, Appl. Catal. A 398 (2011) 1–17.
[45] A. Corma, A.V. Orchilles, Microporous Mesoporous Mater. 35–36 (2000) 21–30.
[46] K. Kubo, H. Iida, S. Namba, A. Igarashi, Microporous Mesoporous Mater. 149 (2012) 126–133.
[47] A. Brait, A. Koopmans, H. Weinstabl, A. Ecker, K. Seshan, J.A. Lercher, Ind. Eng. Chem. Res. 37 (1998) 873–881.
[48] D. Li, F. Li, J. Ren, Y.H. Sun, Appl. Catal. A 241 (2003) 15–24.
[49] S. Sato, R. Takahashi, M. Kobune, H. Gotoh, Appl. Catal. A 356 (2009) 57–63.
[50] A. Martins, J.M. Silva, F.R. Ribeiro, M.F. Ribeiro, React. Kinet. Mech. Cat. 104 (2011) 417–428.
[51] F. Alvarez, F.R. Ribeiro, G. Perot, C. Thomazeau, M. Guisnet, J. Catal. 162 (1996) 179–189.
[52] J. villegas, N. Kumar, T. Salmi, D. Murzin, T. Heikkila, Stud. Surf. Sci. Catal. 158 (2005) 1859–1866.